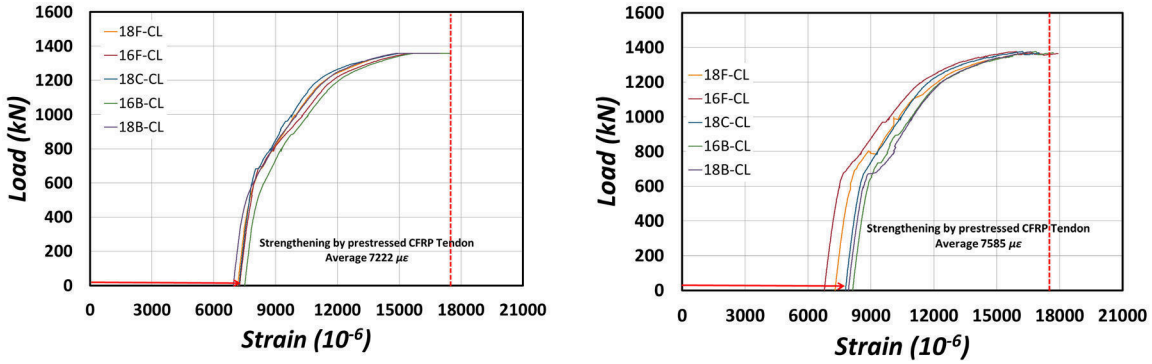

(a) (b)

Fig. 12 — Strain in CFRP tendon according to post-tension loading: (a) Damage-strengthening; (b) No Damage-strengthening [1 kN = 0.22 lb]

Fig. 13 — Failure of the girder specimens

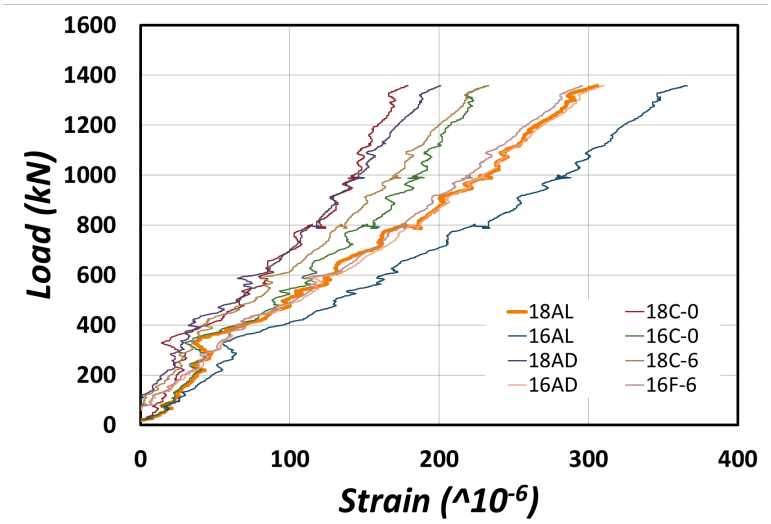

Fig. 14 — Strain distribution in anchored end [1 kN = 0.22 lb]

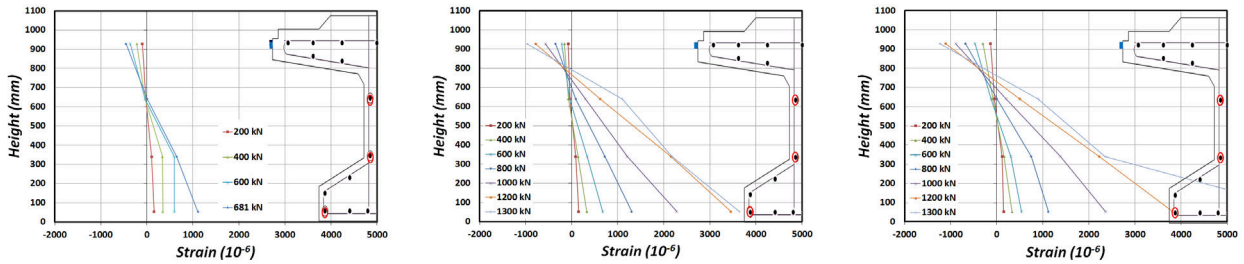

Fig. 15 — Strain distribution per loading stage (central section): (a) Control; (b) Damage-strengthening; (c) No Damage-strengthening. [1 mm = 0.039 in].

Numerical Simulation of AFRP Rod NSM RC Beams under Falling-weight Impact Loading

Masato Komuro, Yusuke Kurihashi, Tomoki Kawarai and Norimitsu Kishi

Synopsis: In order to establish a numerical analysis method to provide an improved estimate of the dynamic response characteristics of reinforced concrete (RC) beams strengthened with near-surface mounted (NSM) Aramid FRP (AFRP) rods under impact loading, a method using fictitious tensile strength of the concrete elements based on an equivalent tensile fracture energy concept (G_f) was proposed. Applying this concept for the concrete elements, an elasto-plastic dynamic response analysis of the RC beams under impact loading was carried out using a fine mesh for a more accurate evaluation of the crack patterns and for a more realistic consideration of the strengthening effects of AFRP rods. The applicability of the method was investigated comparing with the experimental results. Here, configurations of the time histories of the impact force, the reaction force, the mid-span deflection, and crack patterns occurred in the RC beams were used for this investigation. From this study, it was seen that the RC beams strengthened with NSM AFRP rods under falling-weight impact loading can be better simulated using fine meshes with fictitious tensile strength for concrete elements following proposed G_f concept. Here, the case of using a fine mesh having a length of about 6 mm gave appropriate results.

Click here to download accompanying video

Keywords: RC beam; impact load; strengthening method, FRP rod; near-surface mounting (NSM) method, FE analysis; equivalent tensile fracture energy

Masato Komuro is an associate professor of the Civil Engineering Research Unit, College of Environmental Engineering, Muroran Institute of Technology, Japan. He received his PhD from the Muroran Institute of Technology. His research interests include experimental and analytical studies of impact and strengthening problems in steel and concrete structures using more advanced materials.

Yusuke Kurihashi is a lecturer of the Civil Engineering Research Unit, College of Environmental Engineering, Muroran Institute of Technology, Japan. He received his PhD from the Muroran Institute of Technology. His research interests include experimental studies of impact and strengthening problems in concrete structures using more advanced materials.

Tomoki Kawarai is a graduate student of the Muroran Institute of Technology. He is a member of JCI (Japan Concrete Institute). His research interests lie in the numerical simulation of the dynamic response behavior of reinforced concrete and steel structures.

ACI member **Norimitsu Kishi** is the rector of Kushiro College, National Institute of Technology, Japan. He received his PhD from Hokkaido University, Japan. He is a former chairman of the subcommittee for impact problems, JSCE, Japan. His research interests include experimental and analytical studies of impact and strengthening problems in concrete structures using advanced materials.

INTRODUCTION

In recent years, to upgrade the flexural and/or shear load carrying capacity for the existing reinforced concrete (RC) structures, the fiber reinforced polymer (FRP) composites are widely used over the world. In the last two decades, a number of experimental and numerical studies have been carried out to investigate the flexural response of RC beams strengthened with FRP composites [1-6]. The authors have conducted many static loading tests on RC beams strengthened with externally bonded (EB) FRP sheet and/or a near-surface mounted (NSM) FRP rods [7-11]. In addition, the authors numerically analyzed the sheet debonded phenomenon due to a peeling action of the tip of diagonal crack by means of 3D-FE analysis [12]. Many of these studies focused on the behavior of RC structures strengthened with FRP materials under static loading, which have been comprehensively studied and presented in the literatures [13-16]. However, the numerical studies on dynamic behavior and/or responses of the strengthened RC structures with FRP materials under impact loading were relatively limited [17].

On the other hand, in the mountainous areas and/or coastlines in Japan, many rockfall protection RC galleries have been constructed over the highways to protect transportation networks and human lives from falling rocks. However, the impact energy of falling rocks tends to be increased due to aged deterioration and recent weathering of slopes. Therefore, it is necessary to improve the impact-resistant capacity of these RC infrastructures. As a strengthening method for the structures under impact loading, the methods using FRP composites were experimentally investigated by the authors [18, 19]. From the results obtained from these experiments, it is confirmed that the impact-resistant capacity of the RC beams can be better improved applying the Aramid FRP (AFRP) rods NSM method than the EB AFRP one [19]. However, to establish a rational strengthening method for RC beams, not only experimental but also numerical studies should be considered.

From this point of view, in this paper, proposing a numerical analysis method for RC beams strengthened with NSM AFRP rods under falling-weight impact loading, the applicability was investigated comparing with the experimental results [19]. Here, to better simulate dynamic response characteristics of these RC beams, the crack patterns and crack width should be accurately analyzed numerically, and then the interaction between the AFRP rod and the concrete elements should be given more consideration. To accomplish these, an equivalent tensile fracture energy concept for a concrete element [20] was applied in this study. Here, the LS-DYNA code [21] was used in the numerical analysis.

EXPERIMENTAL OVERVIEW

Two types of RC beams were used in this study as shown in Table 1. Beam N was a control beam without strengthening and Beam R were strengthened with NSM AFRP rods. In this table, the nominal names of specimens were designated using the strengthening procedure (N: without strengthening, R: applying the AFRP rod NSM method), and selected falling height (H*n*) (*n*: falling height in metric unit) of the falling weight. The estimated free-falling height (*H'*) was evaluated using the measured falling velocity of the weight just before impacting the upper surface of the beam.

Figure 1 shows the dimensions of the beam, layouts of rebars and of the AFRP rod. The beams have a rectangular cross section of 250 × 200 mm [10 × 8 in] (height × width) and a clear span length of 3.0 m [120 in]. The AFRP

rods were mounted on the tension-side near-surface of the beams leaving 100 mm [4 in] between the supporting point and the end of the rod as shown in Fig. 1. The two deformed steel bars each of diameter ϕ = 19 mm [0.76 in] were placed in the upper and lower fibers, respectively, and were welded to the steel plates of t = 9 mm [0.36 in] thickness at the ends of the beams. Stirrups of diameter ϕ = 10 mm [0.4 in] were placed every 100 mm [4 in]. The yield stresses of the rebars D10 and D19 were 462 and 382 N/mm^2 [67.0 and 55.4 ksi], respectively, obtained from coupon tests as shown in Table 2. Mechanical properties of the AFRP rod used in this study are listed in Table 3, where these values were nominal ones. The compressive strength of the concrete at the commencement of the test is listed in Table 1.

Falling-weight impact tests were conducted by dropping the weight from a prescribed height onto the mid-span of the beam using the impact test apparatus as shown in Fig. 2. The weight consists of a solid steel cylinder installed load-cell and the mass of the falling weight was 300 kg [675 lb]. The RC beams were placed on the supports equipped with load cells for measuring the reaction forces and were clamped at their ends using cross beams to prevent lifting off. The supporting jigs are able to rotate freely while restraining horizontal movement of the beam. The falling weight was dropped vertically via the linear guide rails at the mid-span of the beam.

Here, the time histories of the impact force (P), the reaction force (R), and the mid-span deflection (D) were measured. The axial strain distributions of the AFRP rod were also measured. The mid-span deflection (D) was measured by using a laser-type linear variable displacement transducer (LVDT) with a maximum stroke of 200 mm and a measuring frequency of 915 Hz. These output data were continuously recorded by using digital data recorders with a sampling time of 0.1 ms. After each test, the residual deflection was measured and crack patterns observed on three surfaces of the beam were sketched.

OVERVIEW OF NUMERICAL ANALYSIS

Numerical analysis model

One quarter of each RC beam was three-dimensionally modeled considering two symmetries with respect to the mid-span cross section and the central surface in the widthwise direction of the beam. Figure 3 shows the mesh geometry of the Beam R as an example. In this model, concrete, axial rebars, and AFRP rods were modeled using eight node solid elements and stirrups were modeled using beam elements. The AFRP rods, axial rebars and stirrups were assumed to be bonded perfectly to concrete in this analysis.

The falling weight was modeled precisely following the real shape. In total, about 376,000 nodal points and 351,000 elements are used for modeling the whole structure including the experimental apparatus. To take into account the interactions between the upper surface of the beam near the mid-span area and the impacting surface of the falling weight, and between the upper and lower surfaces of beam near the supporting points and the supporting jigs, the contact-surface elements were defined for those elements in which slide, and contact/non-contact states of these elements can be considered. Friction between each of the two contact-surface elements was ignored. Nodal points along the centerline of the bottom surface of the supporting jig elements were rigidly fixed so as to be able to rotate freely following the actual conditions of the test. For simplicity cracking was evaluated using a smeared cracking model.

The beam was analyzed by inputting an actual impact velocity for all the elements of the falling weight. The damping factor was assumed as h = 0.5% for the fundamental natural frequency of the vertical vibration mode for the analytical model, which was obtained based on the pre-analysis results.

Reference length of concrete element

Firstly, under the conditions for inputting the actual compressive and tensile strengths of the concrete, an appropriate element length of concrete for the analytical model must be determined so as to better predict dynamic responses compared with the experimental results for the control Beam N. The fictitious tensile strength described afterwards should be determined by referring to this element size.

When the element length of concrete was assumed as 25 mm [1 in], comparison of the mid-span deflection between numerical and experimental results for Beam N is shown in Fig. 4. From this figure, it is seen that the experimental results can be satisfactorily simulated using this analytical model. Therefore, the concrete element with a 25 mm [1 in] axial length was defined as the reference one.

This implies that if the length of concrete element is different from that of the reference element for Beam N, the fictitious tensile strength of the concrete should be introduced based on an equivalent tensile fracture energy concept (hereinafter, G_f concept) [20].

When Beam R was modeled using a reference element for concrete, numerical results differed considerably from the experimental results (see, analysis w/o G_f in the case of L = 25 mm [1 in] shown in Fig. 9). This implies that the strengthening effects of the AFRP rod cannot be properly simulated using this model.

This phenomenon may be analyzed as follows: 1) since the smeared crack model is assumed for the concrete elements, the cracks are generated in the elements when the tensile stress reaches the tensile strength; 2) as the results show, the tensile stress in the concrete elements will be lost; 3) thus the tensile stress in the concrete element cannot be transferred to the rod element adjacent to the concrete elements; and 4) if the length of the concrete element were large, AFRP rods would behave so as to be partially debonded and could not effectively strengthen the beam (see, Fig. 5).

Therefore, since numerical crack width is evaluated to be same as the length of concrete element, the concrete elements with smaller length should be used to properly evaluate the dynamic response of the RC beam strengthened with NSM AFRP rods.

From this point of view, in this paper, to accurately evaluate the strengthening effect of AFRP rods, numerical simulations were conducted with varying length of concrete element and using a fictitious tensile strength of concrete based on the G_f concept.

The G_f concept is based on the following assumptions: 1) a smeared crack occurred with the same tensile fracture energy irrespective of the size of element length in the span direction as shown in Fig. 6; 2) the tensile fracture energy of the element i must be set to be equal to that of the reference element; and 3) then the fictitious tensile strength (f_t) is given by following equation [20]:

$$f_t = f_{t0} \cdot \sqrt{\frac{y_0}{y_i}} \tag{1}$$

where the tensile strength of the reference concrete element (f_{t0}) is assumed to be 10% of the compressive strength ($f_c^{'}$) of concrete as mentioned above, y_0 is the reference length (25 mm [1 in]), and y_i is the length of element i in the span direction.

The applicability of this concept was discussed comparing with the experimental results. Figure 7 shows the mesh geometries for an element length of 25mm [1 in], 12.5 mm [0.5 in] and 6.25mm [0.25 in], which are 1/1, 1/2 and 1/4 of the reference length, respectively.

Constitutive model

Figure 8 shows the stress-strain relationships for concrete, rebar and AFRP rod. The relationship for concrete was assumed to be a bilinear model in the region of the compression side and a cut-off model on reaching the tensile strength in the region of tension as shown in Fig. 8(a) [22]. It is assumed that: 1) the yield stress is equal to the compressive strength ($f_c^{'}$); 2) concrete yields on reaching 1500μ strains; 3) yield for concrete is estimated using Drucker-Prager's yield criterion; 4) with the G_f concept, the tensile stress in the element is lost when the calculated negative pressure reaches the fictitious tensile strength of concrete (f_t). The fictitious tensile strength of concrete (f_t) for each selected element length is listed in Table 4.

The stress-strain relationships for axial rebar and stirrups are defined using a bilinear isotropic hardening model as shown in Fig. 8(b). Here, the plastic hardening modulus (H') is assumed to be 1% of the elastic modulus (E_s). Yielding of rebar and stirrups is evaluated following the von Mises yield criterion.

The stress-strain relationship of AFRP rods is assumed to be elastic until the tensile strain reaches the ultimate tensile strain (ε_{ru}) as shown in Fig. 8(c).

The falling weight, supporting jigs, load-cells for measuring reaction forces, and anchor plates for axial rebars were assumed to be elastic according to the experimental observations because no plastic deformation was observed in this test. Their material properties: Young's modulus (E_s), Poisson's ratio (v_s), and density (ρ_s) are assumed to be E_s = 206 kN/mm^2 [30.0×10^3 ksi], v_s = 0.3, and ρ_s = 7.85×10^3 kg/m^3 [5.46 kcf], respectively.

COMPARISON OF NUMERICAL AND EXPERIMENTAL RESULTS

Time histories of impact force, reaction force, and mid-span deflection

Figure 9 shows the comparisons between numerical and experimental results for time histories of the impact force (P), the reaction force (R), and the mid-span deflection (D) of Beam R for the different element lengths and with/without considering the G_f concept. In these figures, origin of the time axis is taken as the time when the falling weight impacts the upper surface of beam.

Figure 9(a) shows the impact force time histories (P) during a 25 ms time interval from the beginning of impact. From these figures, it is observed that: 1) the time histories obtained from the experiment results exhibit a triangular shape with high amplitude and a short time duration of about 1 ms; and 2) the numerical results provide a better simulation irrespective of the with/without consideration of the G_f concept. It implies that the time history of the impact force depends on the local stiffness of concrete elements at the impacted area with falling weight.

Figure 9(b) shows the reaction force time histories (R) during a 100 ms time interval from the beginning of impact. From these figures, it is observed that: 1) the main response obtained from the experimental results is composed of a triangular-shaped component and high-frequency components; 2) a dynamic response with high amplitude is excited over about 40 ms from the beginning of impact; 3) when the G_f concept was not applied, the time duration was more prolonged than that of experimental results irrespective of the size of element length (L); and 4) on the other hand, with an element length 6.25 mm [0.25 in] using the G_f concept, the amplitude and duration of the main response were very similar to those of the experimental results.

Figure 9(c) shows the deflection time histories (D) during 200 ms from the beginning of impact. From these figures, it is observed that: 1) the main response exhibits a half-sine wave, after which the deflection was restrained and the time history exhibits damped sinusoidal shapes; 2) if the G_f concept was not applied, the maximum amplitude tends to be overestimated even though a shorter element length was adopted; 3) on the other hand, if the G_f concept was applied, with an element length 6.25 mm [0.25 in], the maximum amplitude and residual displacement were in good agreement with the experimental results.

Crack patterns

Adopting the constitutive law for concrete applied here, if the major principal stress of the concrete element were zero, this element may be cracked or actually exhibit zero stress. Here, applying this idea, the crack patterns will be predicted.

Figure 10 shows the comparison of the top-, side-, and bottom-surfaces of crack patterns after the test for Beam R between experimental results and numerical results with the G_f concept with an element length L = 25 mm [1 in] and 6.25 mm [0.25 in]. From this figure, it is observed that: 1) in the case of the reference element with L = 25 mm [1 in], the crack pattern on the side-surface of the beam was more widely distributed with horizontal cracks along the AFRP rod comparing with the experimental results; 2) since the crack patterns were generated in the concrete element adjacent to the rod elements, the rod tends to be debonded and the strengthening effects of the rod were not clearly exhibited; and 3) the crack patterns on the top- and bottom-surface of the beam were also much more distributed than those of the experimental results.

On the other hand, with an element length L = 6.25 mm [0.25 in], since the horizontal cracks around the rod on the side-surface of the beam did not appear and the bending and diagonal cracks were developed near the mid-span area, it is seen that these numerical results are in good agreement with the experimental results. Further, the crack patterns on the top- and bottom-surfaces are similar to those obtained from experimental results.

Time history of axial strain in AFRP rod

Figure 11 shows the comparison of the axial strain distribution in the AFRP rod and crack patterns for an element length L = 6.25 mm [0.25 in] with the G_f concept comparing with the experimental results at each time step from the beginning of impact to 30 ms. At 1 ms passed time from the beginning of the impact, it is observed that the strains were distributed like those of the fixed beam with a short span length. As the time proceeds, the span length tends to expand towards the support points. At 5 ms passed time, the strain wave reached the supports and the negative strains near the ends disappeared. Finally, the strain distribution was shifted to that of a simply supported beam.

Comparing strain distributions of the numerical results with the experimental ones, it is observed that the numerical results are similar to those of the experimental results for all time steps except at one point over 2% strain due to fracture of epoxy adhesive. It confirmed that no fracture of the rod occurred after the test. Therefore,

it is seen that the dynamic response of RC beams strengthened with NSM AFRP rods under falling-weight impact loading can be better simulated by applying the G_f concept and using a fine mesh of around 6 mm element length for concrete elements.

CONCLUSIONS

In order to establish a numerical analysis method to accurately simulate the dynamic response characteristics of RC beams strengthened with near-surface mounted (NSM) AFRP rods under impact loading, for a concrete element with a fine mesh, a method using fictitious tensile strength based on an equivalent tensile fracture energy concept (G_f concept) was proposed. Elasto-plastic dynamic response analyses of the RC beams under impact loading were carried out. The applicability of the proposed method was investigated comparing with the experimental results. From this study, the following results were obtained:

1. applying the G_f concept, it is seen that the dynamic response characteristics of the RC beams can be better simulated using a fine mesh of about 6 mm [0.24 in] length in longitudinal direction;

2. crack patterns of the beam and axial strain distributions of AFRP rod can be properly evaluated by applying the proposed method; and

3. the numerical analysis method based on the proposed G_f concept, may be of practical use as a tool for evaluating the dynamic response characteristics of RC beams strengthened with FRP materials.

ACKNOWLEDGMENTS

This work was supported by the Japan Society for the Promotion of Science (JSPS) Grants-in-Aid for Scientific Research C with the Numbers 15K06199 and 17K06527.

REFERENCES

[1] Norris, T., Saadatmanesh, H. and Ehsani, M.R., 1997, “Shear and flexural strengthening of R/C beams with carbon fiber sheets”, *Journal of Structural Engineering*, ASCE, 23(7), 903-911.

[2] Nanni, A, Ludovico, M.D., and Parretti, R., 2004, “Shear strengthening of a PC bridge girder with NSM CFRP rectangular bars”, *Advances in Structural Engineering*, 7, 97-109.

[3] El-Hacha, R, and Rizkalla, S.H., 2004, “Near-surface-mounted fiber-reinforced polymer reinforcements for flexural strengthening of concrete structures”, *ACI Structural Journal*, 101(5), 717-726.

[4] Dai, J.G., Ueda, T., Sato, Y. and Ito, T., 2005, “Flexural strengthening of RC beams using externally bonded FRP sheets through flexible adhesive bonding”, *Proceedings of the International Symposium on Bond Behaviour of FRP in Structures*, December 7-9, Hong Kong, China, 205-213.

[5] Barros, J.A.O., Dias, S.J.E. and Lima, J.L.T., 2007, “Efficacy of CFRP-based techniques for the flexural and shear strengthening of concrete beams”, *Cement and Concrete Composites*, 29(3), 203-217.

[6] Barris, C., Torres, Ll., Turon, A., Baena, M., and Catalan, A., 2009, “An experimental study of the flexural behaviour of GFRP RC beams and comparison with prediction models”, *Composite Structures*, 91(3), 286-295.

[7] Mikami, H., Kishi, N., and Kurihashi, Y., 2000, “Flexural bonding property of FRP sheet adhered to RC beams”, *Proceedings of Congress of IABSE*, Lucerne, Switzerland, Sept.18-21, 380-381.

[8] Kishi, N., Mikami, H., Matsuoka, K.G., and Kurihashi, Y., 2001, “Failure behavior of flexural strengthened RC beams with AFRP sheet*”, Proceedings of FRPRCS-5*, Cambridge, England, July 16-18, 87-95.

[9] Sawada, S., Kishi, N., Mikami, H., and Kurihashi, Y., 2003, “An experimental study on debond-control of AFRPs for flexurally strengthened RC beams”, *Proceedings of FRPRCS-6*, Singapore, July 8-10, 287-296.

[10] Kishi, N., Mikami, H., Kurihashi, Y., and Sawada, S., 2005, “Flexural behavior of RC beams reinforced with NSM AFRP rods”, *Proceedings of the International Symposium on Bond Behaviour of FRP in Structures*, December 7-9, Hong Kong, China, 337-342.

[11] Kurihashi, Y., Kishi, N., and Mikami, H., 2009, “Iterative loading test with constant amplitude for flexural reinforced RC beams with FRP sheet”, *Proceedings of FRPRCS-9*, Sydney, Australia, July 13-15, CD-ROM.

[12] Kishi, N., Zhang, G.F., and Mikami, H., 2005, “Numerical cracking and debonding analysis of RC beams reinforced with FRP sheet”, *Journal of Composites for Construction*, ASCE, 9(6), 507-514.

[13] International Federation for Structural Concrete (fib)., 2001, "Externally bonded FRP reinforcement for RC structures", Bulletin 14.

[14] Concrete Society., 2012, "TR55 Design guidance for strengthening concrete structures using fibre composite materials"

[15] American Concrete Institute., 2017, "440.2R-17: Guide for the Design and Construction of Externally Bonded FRP Systems for Strengthening Concrete Structures"

[16] Aslam, M., Shafigh, P., Jumaat, M.Z., Shah, S.N.R., 2015, "Strengthening of RC beams using prestressed fiber reinforced polymers – A review", *Construction and Building Materials*, 82, 235-256.

[17] Pham, T.M. and Hao, H., 2016, "Review of concrete structures strengthened with FRP against impact loading", *Structures*, 7, 59-70.

[18] Kishi, N., Komuro, M., Kurihashi, Y., and Mikami, H., 2017, "Upgrading effects of near-surface mounting of Aramid fiber reinforced polymer rods on impact resistant capacity of reinforced concrete beams", *6th Interdisciplinary Workshop on Rockfall Protection*, May 22-24, Barcelona, Spain, 149-152.

[19] Kishi, N., Komuro, M., Kurihashi, Y., Mikami, H., and Funaki, T., 2017, "Experimental study on upgrading of impact resistant capacity for RC beams strengthened with NSM-AFRP rods", *Journal of Structural Engineering*, JSCE, 63A, 1188-1200. (in Japanese)

[20] Kishi, N. and Bhatti, A.Q., 2010, "An equivalent fracture energy concept for nonlinear dynamic response analysis of prototype RC girders subjected to falling-weight impact loading", *International Journal of Impact Engineering,* 37, 103-113.

[21] Hallquist, J.O., 2015, "LS-DYNA Version R8 User's Manual", Livermore Software Technology Corporation.

[22] Kishi, N., Khasraghy, S.G., and Kon-no, H., 2011, "Numerical simulation of reinforced concrete beams under consecutive impact loading", *ACI Structural Journal*, 108(4), 444-452.